Nonlinear Critical-Current Thermal Response of an Asymmetric Josephson Tunnel Junction

Claudio Guarcello,[1,*] Alessandro Braggio,[1] Paolo Solinas,[2] and Francesco Giazotto[1]

[1] *NEST, Istituto Nanoscienze-CNR and Scuola Normale Superiore, Piazza San Silvestro 12, I-56127 Pisa, Italy*

[2] *SPIN-CNR, Via Dodecaneso 33, 16146 Genova, Italy*

(Received 9 July 2018; revised manuscript received 5 October 2018; published 1 February 2019)

We theoretically investigate the critical current of a thermally biased superconductor-insulator-superconductor (*S*-*I*-*S*) Josephson junction formed by electrodes made from different Bardeen-Cooper-Schrieffer (BCS) superconductors. The response of the device is analyzed as a function of the asymmetry parameter, $r = T_{c_1}/T_{c_2}$. We highlight the appearance of jumps in the critical current of an asymmetric junction, namely, when $r \neq 1$. In fact, in such a case, at temperatures at which the BCS superconducting gaps coincide, the critical current suddenly increases or decreases. In particular, we thoroughly discuss the counterintuitive behavior of the critical current, which increases by enhancing the temperature of one lead, instead of monotonically reducing. In this case, we find that the largest jump of the critical current is obtained for moderate asymmetries, $r \simeq 3$. In view of these results, the discussed behavior can be speculatively proposed as a temperature-based threshold single-photon detector with photon-counting capabilities, which operates nonlinearly in the nondissipative channel.

DOI: 10.1103/PhysRevApplied.11.024002

I. INTRODUCTION

More than 50 years after its discovery, the Josephson effect [1,2] is still a field that is able to provide intriguing—even unexpected—physical phenomena, from which innovative devices are continuously conceived. This is the case for the plethora of works that have appeared only recently [3–6], based on the earlier intuition that a temperature bias imposed across a Josephson junction (JJ) produces a phase-dependent heat flow through the device [7]. We are dealing with *phase-coherent caloritronics* [5,6,8,9], namely, an emerging research field from which fascinating Josephson-based devices, such as heat interferometers [3,10] and diffractors [4,11,12], heat diodes [13] and transistors [14], solid-state memories [15–17], microwave refrigerators [18], thermal engines [19], thermal routers [20,21], heat amplifiers [22], and heat oscillators [23] have recently been designed and actualized. Even the critical current I_c of a Josephson tunnel junction, namely, the maximum dissipationless current that can flow through the device, deviates from the well-known Ambegaokar-Baratoff relation [24] in the presence of a thermal bias imposed across the junction, namely, as the superconducting electrodes reside at different temperatures, as shown in Fig. 1.

In this work, we explore the distinctive features of the critical current of a thermally biased asymmetric tunnel JJ. We theoretically demonstrate that the critical current I_c of a junction formed by different superconductors shows steeplike variation and is asymmetric in response to a temperature switching. Specifically, we show that the critical current suddenly jumps at specific temperatures at which the Bardeen-Cooper-Schrieffer (BCS) superconducting gaps [25,26] are equal. The abrupt variations are due to the matching in the singularities of the anomalous Green's functions in the two superconductors [25]. This feature is the nondissipative counterpart of the discontinuities discussed in the context of a quasiparticle current flowing through a voltage-biased S_1-I-S_2 junction [25,27] and the heat current flowing through a temperature biased junction [14,28], both of which stem from the alignment of the singularities of the BCS density of states (DOS) in the superconductors [25].

We observe that sudden decreases in the critical current have already been noted, but not extensively discussed so far [14,29]. Additionally, for appropriate parameter values we will show that the critical current behaves counterintuitively, since it increases by enhancing the temperature, instead of decreasing. Furthermore, we study the asymmetry of the critical current with respect to the switching of the temperatures, through the definition of a suitable temperature-switching asymmetry parameter. We also discuss the linear regime in response to a thermal gradient, by studying the first-order coefficients of the critical-current expansion as a function of the average temperature, at a few values of the Dynes parameter.

*claudio.guarcello@nano.cnr.it

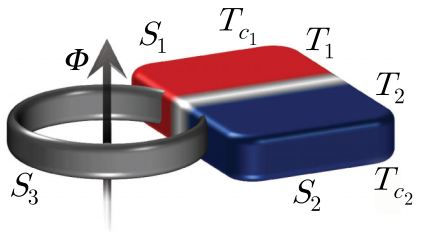

FIG. 1. A schematic illustration of a temperature-biased superconductor-insulator-superconductor (*S-I-S*) Josephson tunnel junction formed by the superconducting leads S_1 and S_2, with critical temperatures T_{c_1} and T_{c_2}, and residing at temperatures T_1 and T_2. The junction is enclosed in a superconducting ring pierced by a magnetic flux Φ, which allows phase biasing of the weak link. The ring is supposed to be made by a third superconductor S_3 with energy gap $\Delta_3 \gg \Delta_1, \Delta_2$ so as to suppress the heat losses.

Finally, according to the steplike behavior of the critical current, we suggest the application of this device as a nondissipative threshold single-photon detector, based on the sudden increase of I_c due to photon-induced heating of one of the electrodes of the junction.

The paper is organized as follows. In Sec. II, we study the behavior of the critical current by nonlinearly varying the temperature of the device and the ratio between the critical temperatures of the two superconductors. In Sec. III, we address the linear approximation in the temperature gradient. We discuss in Sec. IV a possible application of the discussed effects as a single-photon detector. In Sec. V, the conclusions are drawn.

II. THE CRITICAL CURRENT

Here, we explore how the critical current of a temperature-biased *S-I-S* JJ depends on the superconductors composing the device. Indeed, we consider a junction formed by different BCS superconductors, so that we can define an asymmetry parameter

$$r = \frac{T_{c_1}}{T_{c_2}} = \frac{\Delta_{10}}{\Delta_{20}}, \tag{1}$$

where T_{c_j} is the critical temperature and $\Delta_{j0} = 1.764 k_B T_{c_j}$ is the zero-temperature superconducting BCS gap [30] of the jth superconductor (with k_B being the Boltzmann constant).

A Josephson tunnel junction formed by two superconducting leads S_1 and S_2 with energy gaps Δ_1 and Δ_2, residing at temperatures T_1 and T_2 (see Fig. 1), can support a nondissipative Josephson current [25]

$$I_\varphi(T_1, T_2) = I_c(T_1, T_2) \sin\varphi, \tag{2}$$

where φ is the macroscopic quantum phase difference between the superconductors across the junction and $I_c(T_1, T_2)$ is the critical current, which reads [31–34]

$$I_c(T_1, T_2) = \frac{1}{2eR}\left| \int_{-\infty}^{\infty} \{ f(\varepsilon, T_1) \mathrm{Re}[\mathfrak{F}_1(\varepsilon, T_1)] \mathrm{Im}[\mathfrak{F}_2(\varepsilon, T_2)] + f(\varepsilon, T_2) \mathrm{Re}[\mathfrak{F}_2(\varepsilon, T_2)] \mathrm{Im}[\mathfrak{F}_1(\varepsilon, T_1)] \} d\varepsilon \right|. \tag{3}$$

Here, R is the normal-state resistance of the junction, e is the electron charge, $f\left(\varepsilon, T_j\right) = \tanh\left(\varepsilon / 2k_B T_j\right)$, and

$$\mathfrak{F}_j(\varepsilon, T_j) = \frac{\Delta_j\left(T_j\right)}{\sqrt{\left(\varepsilon + i\Gamma_j\right)^2 - \Delta_j^2\left(T_j\right)}} \tag{4}$$

is the anomalous Green's function of the jth superconductor [25], with $\Gamma_j = \gamma_j \Delta_{j0}$ being the Dynes parameter [35]. The so-called Dynes model [35,36] is based on an expression of the BCS DOS that includes a lifetime broadening. It allows to take into account the smearing of the *IV* characteristics of a JJ, i.e., the persistence of a small subgap current at low voltages. In fact, a nonvanishing γ_j effectively introduces states within the gap region, $|\varepsilon| < \Delta_j$, as opposed to the ideal BCS DOS obtained at $\gamma_j = 0$, which instead results in a vanishing DOS within the gap [37,38]. Unless otherwise stated, hereafter we assume that $\gamma_1 = \gamma_2 = \gamma = 10^{-4}$, namely, a value often used to describe realistic superconducting tunnel junctions [13,14,39].

Figure 1 shows a possible experimental realization of the discussed setup where we clearly indicate how to master the phase difference across the device. The thermally biased junction is enclosed, through clean contacts, within a superconducting ring pierced by a control magnetic flux Φ. In this way, we achieve the phase biasing via this external flux, which allows us to thoroughly play with the macroscopic phase difference across the JJ. In fact, neglecting the ring inductance, the phase-flux relation is given by $\varphi = 2\pi\Phi/\Phi_0$ [40], where $\Phi_0 = h/2e \simeq 2 \times 10^{-15}$ Wb is the magnetic flux quantum, with h being the Planck constant. Accordingly, the phase drop across the junction can vary within the whole phase space, i.e., $-\pi \leq \varphi \leq \pi$. The ring is supposed to be made by a third superconductor S_3 with energy gap $\Delta_3 \gg \Delta_1, \Delta_2$ so as to suppress the heat losses due to the Andreev-reflection heat-mirroring effect [41].

A. The nonlinear temperature behavior of I_c

We first study the critical current of the device by choosing the asymmetry parameter r and changing the temperature of S_2 at fixed T_1 for nonlinear temperature regimes.

The behavior of the critical current I_c, in units of $\sqrt{\Delta_{10}\Delta_{20}}/(2eR)$, as a function of the normalized temperature T_2/T_{c_2} at a few values of the normalized temperature

T_1/T_{c_1}, for $r = \{0.5, 1, 2\}$, is shown in Fig. 2. We note that the critical current generally reduces as T_1 increases, an effect that may be naively interpreted as the usual detrimental effect of the temperature on the critical current. Anyway, we will see that for $r \neq 1$, the temperature may affect the critical current in an unexpected way. In fact, we observe that the critical current as a function of T_2 may present a steeplike response. Specifically, for $r \neq 1$, i.e., the asymmetric junction case, the curves may show jumps [see Figs. 2(a) and 2(c)], whereas for a symmetric junction, namely, $r = 1$, the curves present only a change of slope [see Fig. 2(b)]. This distinctive behavior stems from the alignment of the singularities in the Green's functions $\mathfrak{F}_j$ at $\varepsilon = \Delta_j$ when

$$\Delta_1(T_1) = \Delta_2(T_2). \tag{5}$$

In order to correctly interpret this phenomenology, we first discuss the critical currents for $r < 1$, i.e., $r = 0.5$, shown in Fig. 2(a). In this case, the superconducting gap Δ_1 is smaller than Δ_2, namely, $\Delta_1(T) < \Delta_2(T)\ \forall T \in [0 - T_{c_2}]$ [see the inset of Fig. 2(a)], so that for each temperature T_1 there certainly exists a temperature T_2 satisfying Eq. (5). However, this condition is only fulfilled when T_2 is higher than the threshold value $T_2^{\rm th}$ at which $\Delta_2(T_2^{\rm th}) = \Delta_{10}$ (where $\Delta_{10} = \Delta_1(T_1 = 0)$). Specifically, for $r = 0.5$, one obtains $T_2^{\rm th} \simeq 0.91\ T_{c_2}$ [see the dashed lines in the inset of Fig. 2(a)]. Therefore, the sharp jumps in the critical current emerge at $T_2 > T_2^{\rm th}$, namely, at the T_2 values within the shaded region in the inset of Fig. 2(a). We note that the height of the jumps reduces as T_1 increases [42].

In the symmetric case, namely, $r = 1$, shown in Fig. 2(b), the condition (5) can only be satisfied at $T_1 = T_2$. In this case, there is no jump, so that the curves have a change of slope in place of a jump, at $T_1 = T_2$.

Finally, for $r > 1$, i.e., $r = 2$ in Fig. 2(c), $\Delta_1(T) > \Delta_2(T)\ \forall T \in [0 - T_{c_1}]$ [see the inset of Fig. 2(c)], so that the condition (5) is only fulfilled at temperatures T_1 higher than the value $T_1^{\rm th}$ at which $\Delta_1(T_1^{\rm th}) = \Delta_{20}$ (where $\Delta_{20} = \Delta_2(T_2 = 0)$) [see the shaded region in the inset of Fig. 2(c)]. Specifically, for $r = 2$, one obtains $T_1^{\rm th} \simeq 0.91\ T_{c_1}$. Indeed, among those shown in Fig. 2(c), only the curve at $T_1 = 0.94\ T_{c_1}$ shows a jump. Interestingly, in this case the critical current I_c behaves counterintuitively, since when the temperature is raised it increases sharply, undergoing a jump, instead of decreasing monotonically. Moreover, this positive jump becomes higher at a temperature T_1 just above $T_1^{\rm th}$ and reduces when the temperature is further increased. This odd behavior of the critical current can also be anticipated by further inspecting Fig. 2(a), since the point at which the jump is located, i.e., T_2^J, shifts toward higher temperatures as T_1 increases. So, by inverting the roles of T_1 and T_2, the jumps shown in Fig. 2(a) would necessary imply the behavior shown in Fig. 2(c).

We note that in both the $r > 1$ and $r < 1$ cases, the temperature ranges in which the jumps in I_c appear can be enlarged by reducing the temperatures $T_1^{\rm th}$ and $T_2^{\rm th}$, namely, by considering junctions that are less and less asymmetric, i.e., $r \to 1$. Nonetheless, in this case the height of the jumps tends to reduce, up to just vanishing for $r = 1$. Conversely, by increasing the asymmetry between the gaps, namely, for $r \gg 1$ (or $r \ll 1$), we are suppressing one superconducting gap with respect to the other. In these cases, $T_1^{\rm th} \to T_{c_1}$ (or $T_2^{\rm th} \to T_{c_2}$) and the ranges of temperature in which the I_c jumps appear get narrower. Accordingly, since $I_c \to 0$, we expect that, in these regimes also, the height of the I_c jumps will tend to diminish.

In light of this, we investigate the dependence of the height of the critical-current jump, $\Delta I_c^r(T_1)$, on the asymmetry parameter r by varying the temperature T_1. Specifically, we explore the cases for $r > 1$, namely, the cases giving positive jumps of I_c, as already discussed in Fig.2(c). In fact, for $r > 1$, at a temperature $T_2 = T_2^J$ satisfying Eq. (5), the critical current $I_c(T_1 > T_1^{\rm th}, T_2^J)$ suddenly increases. In

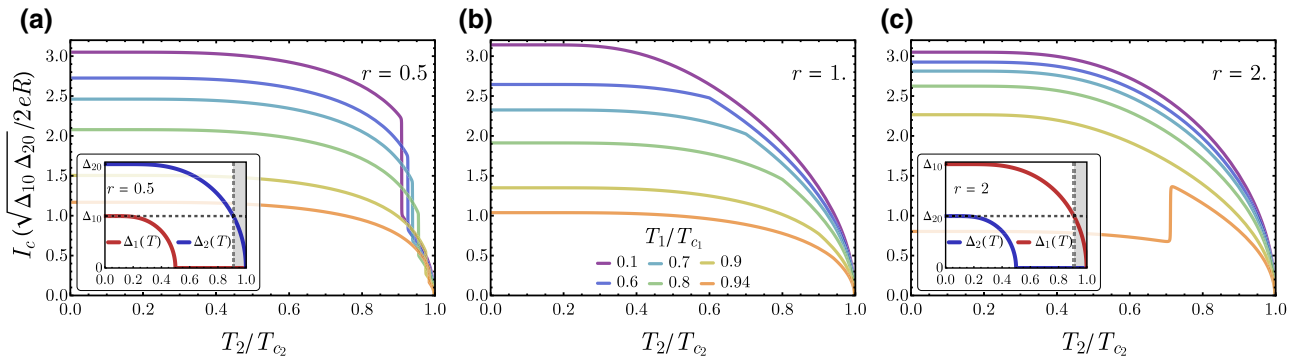

FIG. 2. The critical current, in units of $\sqrt{\Delta_{10}\Delta_{20}}/(2eR)$, as a function of the normalized temperature T_2/T_{c_2} at a few values of the normalized temperature T_1/T_{c_1}, for $r = 0.5$, 1, and 2; see panels (a)–(c), respectively. The insets in panels (a) and (c) show the superconducting gaps Δ_1 and Δ_2 as a function of the temperature T, normalized to $\max\{T_{c_1}, T_{c_2}\}$, for $r = 0.5$ and 2, respectively. The legend in panel (b) refers to all panels.

this case, we additionally observe that I_c has a minimum just before the jump, i.e., for $T_2 < T_2^J$, and a maximum just after the jump, i.e., for $T_2 > T_2^J$. Therefore, we define the height of the critical-current jump as the difference between these maximum and minimum I_c values, namely,

$$\Delta I_c^r(T_1) = \max_{T_2} I_c(T_1, T_2 > T_2^J) - \min_{T_2} I_c(T_1, T_2 < T_2^J), \quad (6)$$

where T_2^J is the temperature T_2 at which the jump occurs, $T_1 > T_1^{\rm th}$, and $r > 1$. The behavior of $\Delta I_c^r(T_1)$ as a function of T_1 at a few values of r is shown in Fig. 3. The vertical dashed-dotted lines indicate the threshold temperatures $T_1^{\rm th}/T_{c_1}$ above which the jumps of I_c appear, calculated at the values of r used in the figure. We observe that, at a given r, $\Delta I_c^r(T_1)$ is maximal for a T_1 just above $T_1^{\rm th}$ and that it reduces linearly as T_1 increases, up to vanishing for $T_1 \to T_{c_1}$. Interestingly, we observe that the maximum value of $\Delta I_c^r(T_1)$, calculated as $\Delta I_c^{\rm max} = \max_{T_1} \Delta I_c^r(T_1)$, behaves nonmonotonically as $r > 1$ increases, approaching zero for $r \to 1$ and $r \gg 1$ and reaching a maximum for $r \simeq 3$, as shown in the inset of Fig. 3. Accordingly, the highest I_c jump is obtained for $T_{c_1} \simeq 3T_{c_2}$.

To have an idea of the situation in which the present effect can be observed, we assume a JJ with a barrier resistance of $R = 100\ \Omega$ between, for instance, Nb ($T_{c_1} = 9.2$ K) and Ta ($T_{c_2} = 4.4$ K), corresponding to an asymmetry parameter of $r \approx 2$. In this case, one finds a jump of $\Delta I_c^{r=2} \simeq 1.2\sqrt{\Delta_{10}\Delta_{20}}/(2eR) \simeq 5.8\ \mu$A when the maximal critical current at low temperature is $I_{c,\max}^{r=2} \simeq 3.05\sqrt{\Delta_{10}\Delta_{20}}/(2eR) = 14.5\ \mu$A [see Fig. 2(c)]. Nonetheless, we observe that in this case the range of T_1 at which the behavior of I_c emerges is very close to the critical temperature.

In the previous discussion, we analyze the jump for $r > 1$, although one can also easily generalize the previous results to the $r < 1$ case, due to the discussed symmetry between the $r < 1$ and $r > 1$ cases, by exchanging the role of the temperatures T_1 and T_2. In particular, for $r < 1$, the jump height will be a maximum for $r \simeq 1/3$. In this case, the value of T_2 at which the jump appears is really close to the critical temperature T_{c_2}, as can easily be seen by comparing Fig. 2(a) with Fig. 2(c).

The impact of the Dynes parameter γ on the critical current is highlighted in Fig. 4. In this figure, the behavior of I_c, in units of $\sqrt{\Delta_{10}\Delta_{20}}/(2eR)$, is shown, as a function of T_2/T_{c_2} at a few values of γ, for $r = 0.5$ and $T_1/T_{c_1} = 0.1$. Specifically, we demonstrate how the critical current changes by varying γ in the neighborhood of a jump. We observe that the higher the γ value, the smoother is the I_c [43].

In Sec. IV, we will discuss some possible applications of this device, but certainly the sharpness of the jump is an important figure of merit, which is potentially connected to the sensitivity of the junction to small temperature variations around the operating point T_2^J. Higher sensitivities in temperature can be obtained by maximizing the jump sharpness, i.e., by increasing the current jump height ΔI_c and/or by minimizing the Dynes parameter [37]. We note that, from the perspective of detecting small variations of T_2, it is more convenient to consider the case where the jump, as a function of T_2, is positive, as shown in Fig. 2(c) for $r > 1$, since the normalized temperature T_2^J/T_{c2} is smaller than in the case with $r < 1$. This means keeping the superconducting electrode with the higher T_c at a temperature quite close to the critical value and leaving the

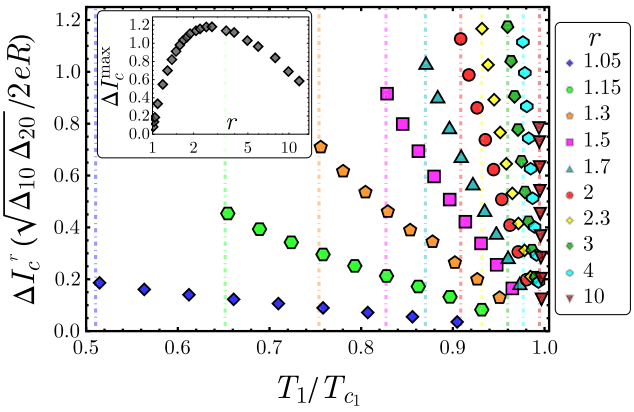

FIG. 3. The height of the critical-current jump [see Eq. (6)], in units of $\sqrt{\Delta_{10}\Delta_{20}}/(2eR)$, as a function of T_1/T_{c_1} at a few values of $r \in]1\text{–}10]$. The vertical dotted lines indicate the threshold temperatures $T_1^{\rm th}/T_{c_1}$ above which the jumps of I_c appear, calculated at the values of r used in the figure. The inset shows the maximum value of ΔI_c^r, i.e., $\Delta I_c^{\rm max} = \max_{T_1} \Delta I_c^r(T_1)$, in units of $\sqrt{\Delta_{10}\Delta_{20}}/(2eR)$, as a function of r.

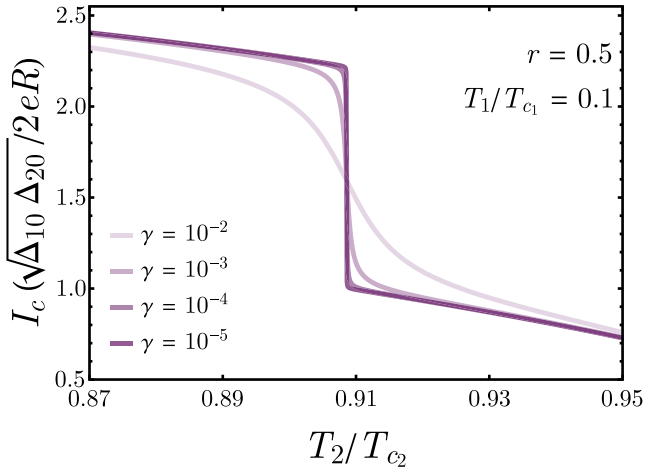

FIG. 4. The critical current, in units of $\sqrt{\Delta_{10}\Delta_{20}}/(2eR)$, as a function of T_2/T_{c_2}, at a few values of the Dynes parameter γ, for $r = 0.5$ and $T_1/T_{c_1} = 0.1$.

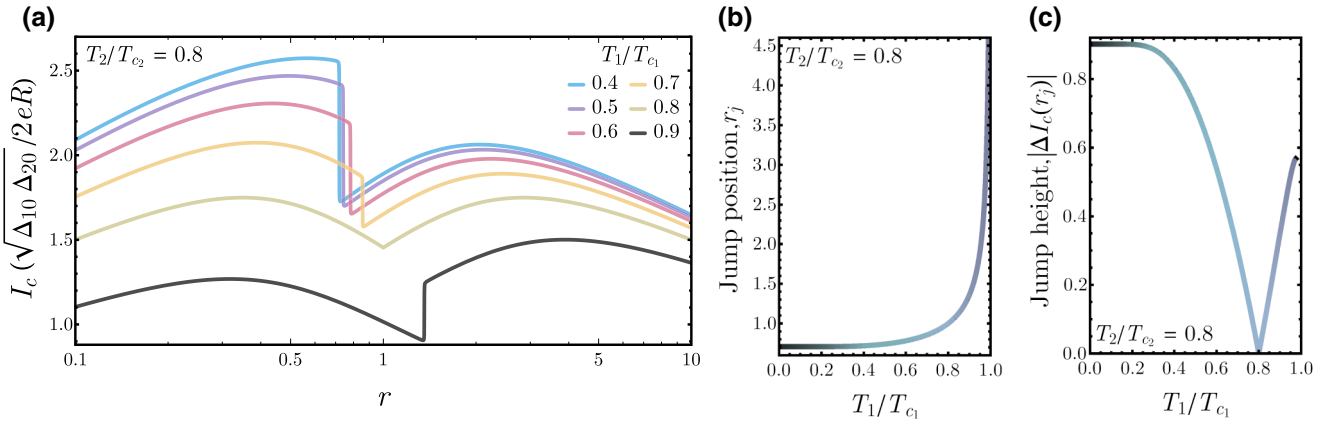

FIG. 5. (a) The critical current, in units of $\sqrt{\Delta_{10}\Delta_{20}}/(2eR)$, as a function of the asymmetry parameter r, at a few values of the normalized temperature T_1/T_{c_1} and $T_2/T_{c_2} = 0.8$. (b),(c) The position and height of the critical-current jump as a function of T_1/T_{c_1} for $T_2/T_{c_2} = 0.8$.

temperature of the other electrode free to range around the jump temperature T^J.

As discussed so far, the critical current strongly depends on the asymmetry parameter r. In this regard, in Fig. 5(a) we illustrate the behavior of the critical current I_c, in units of $\sqrt{\Delta_{10}\Delta_{20}}/(2eR)$, as a function of r, at a few values of the normalized temperature T_1/T_{c_1} and $T_2/T_{c_2} = 0.8$. We observe that these curves may also show a jump, except for the curve at $T_1/T_{c_1} = T_2/T_{c_2}$. In the latter case, I_c shows a cusp in $r = 1$, since its slope suddenly changes from negative to positive around $r = 1$, and it is symmetric, on a semilogarithmic plot, with respect to this point. The position r_j of the jump of I_c changes with the temperature T_1/T_{c_1} and can be estimated through Eq. (5). In Fig. 5(b), we display the jump position r_j as a function of T_1/T_{c_1}, for $T_2/T_{c_2} = 0.8$. Additionally, the height of the I_c jumps, $|\Delta I_c(r_j)|$, as a function of T_1/T_{c_1}, is shown in Fig. 5(c) for $T_2/T_{c_2} = 0.8$. We observe that $\Delta I_c(r_j)$ has a plateau at low T_1's and that it decreases as T_1 increases, up to vanishing at $T_1 = T_2$, whereupon it increases again.

Finally, with the aim of quantifying the asymmetry of the critical current with respect to the switching of the temperatures T_1 and T_2, keeping the structural asymmetry r fixed, we define the temperature-switching asymmetry parameter $\mathcal{R}$:

$$\mathcal{R}(\%) = \frac{I_c(T_1, T_2) - I_c(T_2, T_1)}{I_c(T_2, T_1)} \times 100. \qquad (7)$$

This parameter synthetically describes how the structural asymmetry r induces strongly asymmetrical behavior on the nondissipative branch represented by an asymmetry of the critical current with the exchange of the temperatures of the superconducting leads. In the density plot shown in Fig. 6(a), we display the behavior of $\mathcal{R}$ as a function of T_1/T_{c_1} and T_2/T_{c_2}, for $r = 0.5$. We observe that $\mathcal{R}$ also shows jumps, just corresponding to the I_c jumps previously discussed in Fig. 2. Furthermore, the sign of $\mathcal{R}$ switches in correspondence to a jump. If $|\mathcal{R}|$ is a maximum, this means that the variation of I_c due to the switching of the temperatures is also maximal. Conversely, if $\mathcal{R} = 0$, the critical current is symmetric with respect to a temperature switch, although the system is intrinsically asymmetric, since $r \neq 1$. Three selected profiles of $\mathcal{R}$ as a function of T_2/T_{c_2} for different values of T_1/T_{c_1} are also shown in Fig. 6(b). The situations plotted in this figure correspond to the colored dashed lines in Fig. 6(a). For $T_1 < T_1^{\text{th}}$, by varying T_2/T_{c_2} we note that $\mathcal{R}$ undergoes only one jump at a temperature $T_2 > T_2^{\text{th}}$ [see the curves at $T_1/T_c = 0.2$ and 0.7 in Fig. 6(b)]. In these cases, $\mathcal{R}$ increases monotonically before the jump, whereas it becomes negative and decreases monotonically after the jump. Moreover, the height of these jumps reduces as T_1 increases. Conversely, at a temperature $T_1 > T_1^{\text{th}}$, we observe two jumps in $\mathcal{R}$ [see the curve at $T_1/T_c = 0.92$ in Fig. 6(b)], since both $I_c(T_1, T_2)$ and $I_c(T_2, T_1)$ behave discontinuously at some values of T_2. Also, in this case $\mathcal{R}$ becomes negative after a jump.

The behavior of $\mathcal{R}$ as a function of T_2/T_{c_2} at a few values of the asymmetric parameter $r < 1$ is shown in Fig. 6(c), at $T_1/T_c = 0.2$. We note that the lower the value of r, the higher are both the temperature at which $\mathcal{R}$ changes abruptly and the height of its jump. Conversely, in the symmetric case, $r = 1$, the critical current is symmetric in the switching of the temperatures, namely, $I_c(T_1, T_2) = I_c(T_2, T_1)$, so that $\mathcal{R} = 0\ \forall T_1, T_2$.

III. THE LINEAR-RESPONSE APPROXIMATION

In this section, we analyze the variation of the critical current for small temperature differences between the two superconductors. Our aim is to quantify how small temperature differences will affect the nondissipative regime in the presence of a structural asymmetry, $r \neq 0$, in the junction.

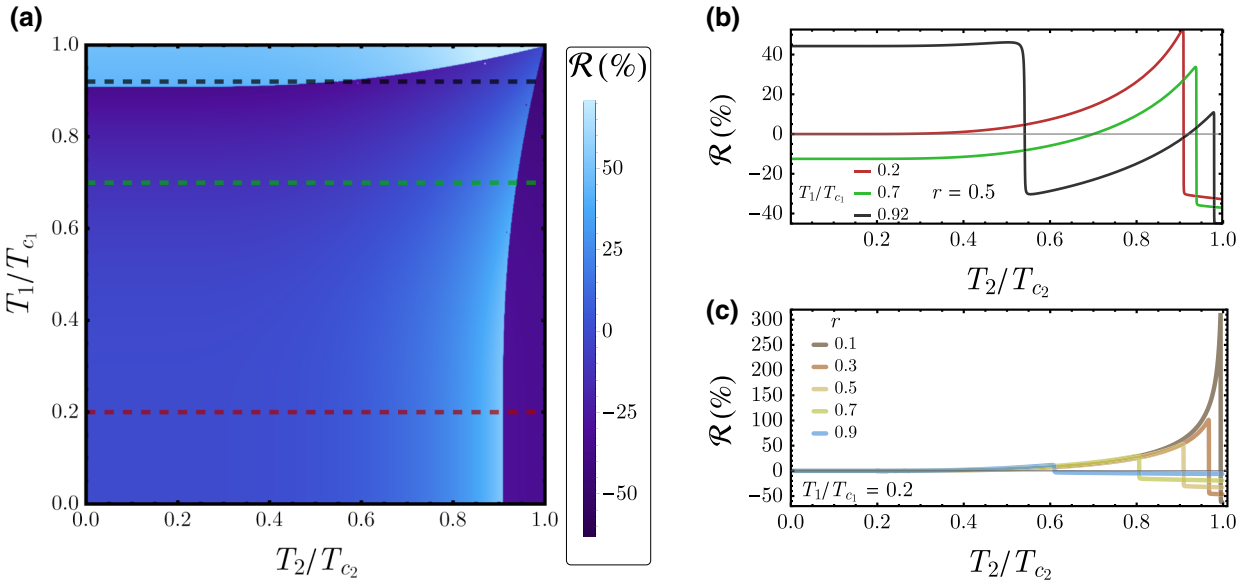

FIG. 6. (a) The parameter $\mathcal{R}$ [see Eq. (7)], as a function of T_1/T_{c_1} and T_2/T_{c_2}, for $r = 0.5$. (b), Profiles of $\mathcal{R}$ vs T_2/T_{c_2}, for $T_1/T_{c_1} = \{0.2, 0.7, 0.92\}$ and $r = 0.5$, corresponding to the colored dashed lines in (a). (c) The parameter $\mathcal{R}$ [see Eq. (7)], as a function of T_1/T_{c_1}, at a few values of r and $T_2/T_{c_2} = 0.2$.

We assume that $T_1 > T_2$, so that we can define T and δT such that $T_1 = T + \delta T/2$ and $T_2 = T - \delta T/2$ and we can investigate the linear-response approximation by imposing $\delta T = T_1 - T_2 \ll T = (T_1 + T_2)/2$.

The critical current [see Eq. (3)] depends on the lead temperatures through both the statistical factors $f_j \equiv f\left(\varepsilon, T_j\right)$ and the self-consistent superconducting gap $\Delta_j \equiv \Delta_j(T_j)$ (with $j = 1, 2$). The linear behavior in δT of the critical current $I_c = \int_{-\infty}^{+\infty} d\epsilon J_c(\epsilon)$ can easily be written as

$$\frac{\delta I_c}{\delta T} = \int_{-\infty}^{+\infty} d\epsilon \left(\sum_i \underbrace{\left.\frac{\delta J_c(\epsilon)}{\delta f_i}\right|_{\Delta_j} \frac{\partial f_i}{\partial \delta T}}_{\alpha_1} + \underbrace{\left.\frac{\delta J_c(\epsilon)}{\delta \Delta_i}\right|_{f_j} \frac{\partial \Delta_i}{\partial \delta T}}_{\alpha_2} \right), \tag{8}$$

where in the first term (α_1) we consider only the temperature variation of the statistical weights f_i and in the second (α_2) the temperature variation of the gaps Δ_i. Finally, the critical current can be written as

$$I_c\left(T, \delta T\right) \simeq I_c(T, 0) + \alpha_1(T)\delta T + \alpha_2(T)\delta T, \tag{9}$$

where

$$I_c(T, 0) = \frac{1}{2eR}\left| \int_{-\infty}^{\infty} f\left(\varepsilon, T\right) \mathrm{Im}\left[\mathfrak{F}_1(\varepsilon, T)\mathfrak{F}_2(\varepsilon, T)\right] d\varepsilon \right| \tag{10}$$

coincides exactly with the well-known Ambegaokar-Baratoff relation [25]. Therefore, the linear contribution to the critical current can be seen as a correction to the usual relation, Eq. (10), due to the asymmetry of the junction and the temperature gradient. This contribution is determined by two different terms, α_1 and α_2 [see Eq. (8)]. The former is associated with the variation of the electron distribution, assuming temperature-independent gaps. On the other hand, the latter, α_2, is computed by considering only temperature variations of the superconducting gaps included in the anomalous Green's functions $\mathfrak{F}_j$ [see Eq. (4)].

According to the modulus in Eq. (3), if we recast the critical current as $I_c = |\mathfrak{I}_c|$, its derivative can be written as $\partial I_c/\partial \delta T = \mathrm{sgn}(\mathfrak{I}_c)(\partial \mathfrak{I}_c/\partial \delta T)$. Then the coefficient α_1 reads

$$\alpha_1(T) = \frac{\mathrm{sgn}(\mathfrak{I}_c)}{8eRk_BT^2} \int_{-\infty}^{\infty} d\varepsilon\, \varepsilon \frac{\mathrm{Im}\left[\mathfrak{F}_1(\varepsilon, T)\mathfrak{F}_2^*(\varepsilon, T)\right]}{\cosh^2(\varepsilon/2k_BT)}, \tag{11}$$

where it is easy to recognise the derivative contribution of f_i as being taken directly from Ambegaokar-Baratoff [Eq. (10)]. On the other hand, by expanding the anomalous terms in Eq. (3) to the first order in δT, the coefficient α_2 can be expressed as

$$\alpha_2(T) = \frac{\mathrm{sgn}(\mathfrak{I}_c)}{4eR} \int_{-\infty}^{\infty} d\varepsilon f\ (\varepsilon, T) \times \sum_i (-1)^{i-1} \frac{\Delta_i'(T)}{\Delta_i(T)} \beta_i\left(\varepsilon, T\right), \tag{12}$$

where $\Delta_i'(T)$ is the derivative with respect to T of the ith superconducting gap and $\beta_j\left(\varepsilon, T\right) = \mathrm{Im}\left(\mathfrak{F}_1\mathfrak{F}_2\right) \mathfrak{N}_j^2 - \frac{i}{2}\mathrm{Re}\left(\mathfrak{F}_1\mathfrak{F}_2\right) \mathfrak{F}_j^2$, with $\mathfrak{N}_j\left(\varepsilon, T\right) = (\varepsilon + i\Gamma_j)/$

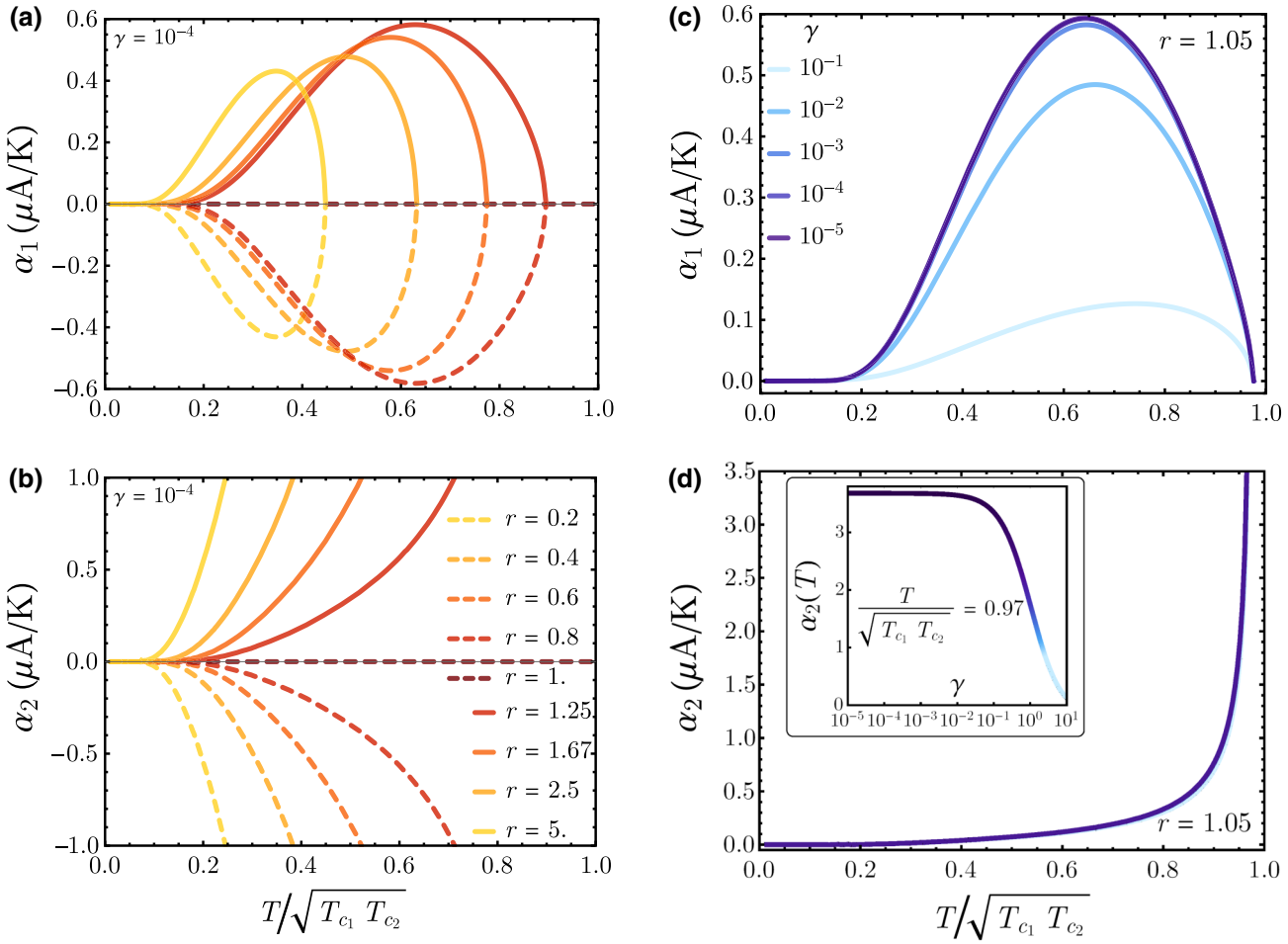

FIG. 7. (a),(b) The coefficients α_1 and α_2 [see Eqs. (11) and (12)] as a function of the normalized temperature $T/\sqrt{T_{c_1}T_{c_2}}$, for $\gamma = 10^{-4}$ and several values of r. The legend in panel (b) refers to both panels. (c),(d) The coefficients α_1 and α_2 as a function of the normalized temperature $T/\sqrt{T_{c_1}T_{c_2}}$ for several γ and $r = 1.05$. In the inset of panel (d) is shown α_2 as a function of γ for $T/\sqrt{T_{c_1}T_{c_2}} = 0.97$ and $r = 1.05$. The legend in panel (d) refers to both panels.

$\sqrt{(\varepsilon + i\Gamma_j)^2 - \Delta_j^2(T)}$. We see that the gaps only affect the linear coefficient α_2 via their logarithmic derivatives $\Delta_i'(T)/\Delta_i(T)$.

We note that both α_1 and α_2 are linear coefficients of the dissipationless regime, so they can only be defined for $T \leq \min\{T_{c_1}, T_{c_2}\}$. In order to efficiently represent these terms for different structural asymmetries r, it is convenient to normalize the temperature with respect to $\sqrt{T_{c_1}T_{c_2}}$. Therefore, one can easily verify that the linear coefficients are only defined for $T/\sqrt{T_{c_1}T_{c_2}} \leq \min\{\sqrt{r}, 1/\sqrt{r}\}$.

The behavior of the coefficients α_1 and α_2, as a function of the normalized temperature $T/\sqrt{T_{c_1}T_{c_2}}$ for $r \in [0.2\text{–}5]$, is shown in Figs. 7(a) and 7(b), respectively. Hereafter, we will assume a Nb ($T_{c_1} = 9.2$ K) electrode S_1 and we will suppose that we are able to set the gap of S_2 at will, in order to get the appropriate value of the asymmetry parameter r. The barrier resistance is set to $R = 100\ \Omega$, which results in a junction that, for the symmetric case $r = 1$, has a low-temperature critical current of approximately 22 μA.

First, we observe that both α_1 and α_2 vanish for $r = 1$ [see Figs. 7(a) and 7(b), respectively], namely, there is no linear contribution to the critical current with the temperature gradient in the symmetric case. Conversely, both coefficients are positive for $r > 1$ and negative for $r < 1$. This remark can be rationalized by observing that the critical current scales roughly according to the geometric mean of the superconducting gaps $\sqrt{\Delta_1(T_1)\Delta_2(T_2)} = \sqrt{\Delta_1(T + \delta T/2)\Delta_2(T - \delta T/2)}$. Interestingly, the δT derivative of this quantity is positive for $r > 1$ and negative for $r < 1$. This shows that the sign of $\delta I_c/\delta T$ in a JJ under a small temperature gradient δT directly reflects on the structural asymmetry r in the junction.

We observe that α_1 behaves nonmonotonically [see Fig. 7(a)], since, for $r < 1$, it starts from zero, reaches a minimum, and then vanishes at $T/\sqrt{T_{c_1}T_{c_2}} = \sqrt{r}$, i.e., at

$T = T_{c_1}$. Similarly, for $r > 1$ it starts from zero, reaches a maximum, and finally vanishes at $T/\sqrt{T_{c_1}T_{c_2}} = 1/\sqrt{r}$, i.e., at $T = T_{c_2}$. For low temperatures, the behavior of α_1 is ruled by the exponential suppression of the hyperbolic contribution for $T \to 0$. Instead, for $T/\sqrt{T_{c_1}T_{c_2}} \to \min\{\sqrt{r}, 1/\sqrt{r}\}$, namely, for $T \to \min\{T_{c_1}, T_{c_2}\}$, the product $\sqrt{\Delta_1(T)\Delta_2(T)}$ vanishes, so that α_1 goes to zero according to the BCS temperature dependence of $\Delta_1(T)$ or $\Delta_2(T)$. Moreover, we observe that the maximum value of $|\alpha_1|$ increases if $r \to 1$. This apparently odd result is consistent with the fact that when $T_1 \approx T_2$, the critical current is not analytic in the asymmetry parameter r, as implied by the cusp shown in Fig. 5(a) for $r = 1$ and $T_1 = T_2$.

Conversely, α_2 behaves monotonically [see Fig. 7(b)]. Specifically, it vanishes rapidly at $T \to 0$ and diverges at $T/\sqrt{T_{c_1}T_{c_2}} \to \min\{\sqrt{r}, 1/\sqrt{r}\}$. The low-temperature behavior of α_2 is mainly governed by the gap logarithmic derivatives, the superconducting gap being roughly constant at $T \lesssim T_{c_j}/4$ so that $\Delta_j{}'(T) \to 0$ at $T \to 0$. Instead, for $T \to \min\{T_{c_1}, T_{c_2}\}$, although $\Delta_j(T) \to 0$, we observe that the logarithmic derivative diverges, making α_2 also diverge.

Interestingly, we observe that the coefficients α_1 and α_2 behave quite differently when the Dynes parameter γ is varied, as is clearly shown in Figs. 7(c) and 7(d) for a few values of $\gamma \in [10^{-5}$–$10^{-1}]$ and $r = 1.05$. We observe that α_1 is strongly affected by γ, since it reduces significantly as γ increases, up to becoming even 5 times lower passing from $\gamma = 10^{-5}$ to $\gamma = 10^{-1}$ [see Fig. 7(c)]. Conversely, the coefficient α_2 is practically independent of γ, as is shown in Fig. 7(d). Interestingly, we observe that to appreciate concrete variations in α_2, we should consider much higher, unrealistic values of γ [see the curve shown in the inset of Fig. 7(d) obtained at $T/\sqrt{T_{c_1}T_{c_2}} = 0.97$].

IV. DISCUSSION: A POSSIBLE APPLICATION FOR SINGLE-PHOTON SENSING

The physical effect described so far could readily find an application in several contexts. For instance, this device can be used as the Josephson counterpart of a thermal-current rectifier, which exploits the I_c drop upon temperature-bias reversal. Interestingly, several examples of thermal rectifiers, namely, structures allowing high heat conduction in one direction but suppressing thermal transport upon a temperature switch, based on Josephson junctions [13,44–46], phononic devices [47–49], and quantum dot [50], have also recently been conceived.

Alternatively, a nondissipative single-photon detector [51–57] based on a temperature-biased asymmetric Josephson tunnel junction might be conceived. The development of superconducting sensors is a subject of growing interest recently, since the use of superconducting devices working at cryogenic temperatures offers some advantages. To name just a few, they assure a significant suppression of the heat leakage [51,58–60] and a vanishingly small Johnson noise [61], since they operate in the nondissipative regime.

The setup that we are proposing resembles a superconducting tunnel junction (STJ) detector in which a tunnel Josephson junction is exploited in the dissipative regime [62–64]. Conversely, in our proposal we operate the tunnel junction in the dissipationless regime without involving any quasiparticle charge current [65].

This single-photon detector implementation is worth discussing in more detail. In the proposed device concept, the measurable abrupt increase of the critical current, as determined by the enhancement of the temperature of the absorbing superconducting layer, could be exploited to detect radiation. In such a setup, the photon is supposed to be absorbed in an electrode with a small volume (i.e., with a small heat capacitance), for instance, the electrode S_2, to allow its temperature to change effortlessly due to a small energy absorption. The other electrode, i.e., S_1, is instead supposed to have a large volume and is endowed with a heating probe that continuously injects heat, in order to keep its temperature T_1 as constant as possible. At the same time, the system is assumed to be in good thermal contact with a phonon bath.

The temperature of electrode S_2 is initially kept close to the threshold value T_2^J. Due to the photon absorption and the resulting temperature increase, the critical current can jump. Then, in such a detector, the choice of the working temperature, $T_2(0)$, is an essential consideration. In particular, $T_2(0)$ must be chosen close enough to T_2^J so that the incoming photon can induce the transition. At the same time, if $T_2(0)$ is too close to T_2^J, unavoidable thermal fluctuations in the superconductor could trigger a faulty detector reaction. For this reason, the analysis of the thermal fluctuations is of crucial importance in estimating the feasibility of the detector. Indeed, first we need the temperature separation $\Delta T_2 = T_2^J - T_2(0)$ to be much larger than the possible temperature fluctuations, in order to reduce the dark counts to a minimum. At the same time, reducing the separation ΔT_2 increases the sensitivity to low-energy photons. The thermodynamic temperature fluctuations can be estimated as [56,66]

$$\delta T = \sqrt{\frac{k_B T^2}{C_j(T)}}. \tag{13}$$

Here, $C_j(T) = T\partial \mathcal{S}_j/\partial T$ is the electronic heat capacity of the superconductor S_j, where $\mathcal{S}_j(T)$ is its electronic entropy and is given by [18,67]

$$\mathcal{S}_j(T) = -4k_B V_j N_{F,j} \int_{-\infty}^{\infty} f(\varepsilon, T) \ln[f(\varepsilon, T)] \mathcal{N}_j(\varepsilon, T) d\varepsilon. \tag{14}$$

Here, V_j is the volume, $N_{F,j}$ is the quasiparticle DOS at the Fermi energy, $f(E,T)$ is the Fermi distribution function, and $\mathcal{N}_j(\varepsilon,T) = |\mathrm{Re}[(\varepsilon + i\Gamma_j)/\sqrt{((\varepsilon + i\Gamma_j)^2 - \Delta_j(T)^2)}]|$ is the smeared BCS DOS of S_j. Since $\delta T \propto V_j^{-1/2}$, we observe that the lower the electrode volume, the higher are the thermal fluctuations. Therefore, in the design of the detector, care should be taken to fully determine the volume of the absorber, since a smaller volume may be beneficial for sensitivity at low energies but also potentially detrimental due to the increase of the thermodynamic fluctuations.

Hereafter, we refer to a device configuration previously used as an example, namely, a junction with electrodes S_1 and S_2, respectively, made from Nb ($T_{c_1} = 9.2$ K) and Ta ($T_{c_2} = 4.4$ K), so that $r \approx 2$. This material selection has already demonstrated a high quantum efficiency in absorbing photons from infrared (IR) to ultraviolet (UV) frequencies [64]. In the inset of Fig. 8, we show the critical current of a Nb/Ta junction with $R = 100\ \Omega$ as a function of T_2. In this case, the critical current jumps at $T_2 \simeq 2.54$ K. The behavior of δT, as a function of the temperature of the Ta electrode with $V_2 = 0.01\ \mu\mathrm{m}^3$, $T_{c_2} = 4.4$ K, and $N_{F,2} = 10^{47}\ \mathrm{J}^{-1}\mathrm{m}^{-3}$, is shown in Fig. 8. We observe that in this case the fluctuations are vanishingly small over a large range of temperatures. For instance, by assuming that one is to working at 2.5 K, one obtains $\delta T \simeq 5$ mK. This means, for instance, that a working temperature that is distant just $\Delta T_2 = 50$ mK from the threshold value could safely prevent an unreliable absorber-temperature readout. The red dashed line in the inset of Fig. 8 indicates the working temperature obtained by choosing $\Delta T_2 = 50$ mK.

We observe that in the single-photon detection mode, the proposed detector is characterized by a "dead time" during which it cannot be used to reveal a following incident photon. After an absorption, the temperature T_2 increases, reaching a maximum during a jitter time and then, due to the thermal contact with the phonon bath, the electrode S_2 recovers its initial steady temperature. However, once a transition induced by a photon with sufficient energy has occurred, a further photon-induced temperature increase will not induce another I_c jump unless the system has already switched back to its idle state. During the thermal evolution following a photon absorption, the condition $T_2 = T_2^J$ at which I_c jumps is satisfied twice. The separation in time between these subsequent photon-induced I_c jumps can be used to define the dead time of the device. Since the maximum temperature reached by S_2 depends on the absorbed energy, the photon frequency could be directly inferred from this dead time, which can be reduced by device and fabrication optimization. In fact, since the thermalization time can be estimated as $\tau_{\mathrm{th}} = C_j/G$ [21] (with G being the total thermal conductance of the JJ), the energy excess due to the photon absorption could be released more quickly by allowing the superconductor S_2 to be strongly coupled to the thermal phononic bath. The possibility of working at temperatures of the order of $T_c/2$ guarantees a good e-ph coupling and then a quite short dead time in comparison with other detectors working at $T \ll T_c$. Furthermore, in the case of monochromatic radiation, our device shows intriguing photon-number-resolving detection capabilities, since the dead time depends directly on the absorbed energy.

The possibility of distinguishing photons with different frequencies would allow us to use the device as a calorimeter. To estimate the performance of a calorimeter, the relevant figure of merit is the resolving power, which is calculated in the idle state in the absence of photonic excitation, and reads as follows [52,57]:

$$\frac{h\nu}{\Delta E} = \frac{h\nu}{4\sqrt{2\ln 2}\sqrt{k_B T^2 C(T)}}, \tag{15}$$

where T is the steady temperature of the absorber, ν is the photon frequency, and ΔE is the intrinsic energy resolution calculated as the full width at half maximum for a calorimeter with a white-noise spectrum [8,52]. Figure 9(a) shows the resolving power as a function of the photon frequency, ν, at a few temperatures of the Ta electrode with volume $V_2 = 0.01\ \mu\mathrm{m}^3$. We observe that the resolving power obviously increases linearly with the photon frequency. The horizontal dashed line indicates unitary resolving power. We note that at 0.6 K, a resolving power exceeding 1 results in the whole range of frequencies shown in Fig. 9(a) (IR to UV light spectrum). Instead, for $T_2 = 2.5$ K, namely, the working temperature previously discussed (see the inset of Fig. 8), we only obtain $h\nu/\Delta E > 1$ at frequencies above 100 THz. This means that a Nb/Ta-based detector, with the chosen detection volume V_2, residing at a temperature $T_2 = 2.5$ K, could work properly as a calorimeter for frequencies $\nu \gtrsim 100$ THz.

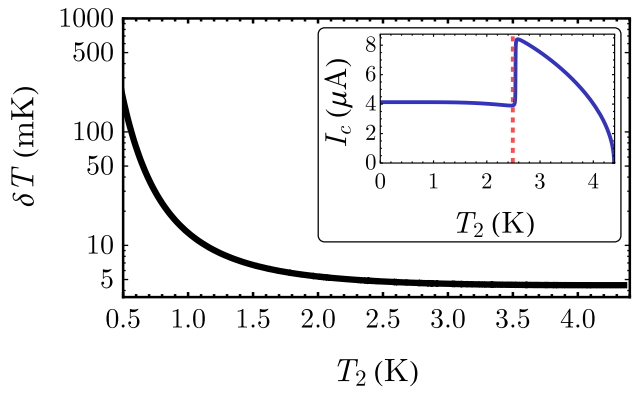

FIG. 8. The thermodynamic temperature fluctuations δT as a function of the temperature T_2 of a Ta electrode with volume $V_2 = 0.01\ \mu\mathrm{m}^3$, $T_{c_2} = 4.4$ K, and $N_{F,2} = 10^{47}\ \mathrm{J}^{-1}\,\mathrm{m}^{-3}$. In the inset is shown the critical current, I_c, as a function of T_2, at $T_1/T_{c_1} = 0.93$, for a Nb/Ta junction with $R = 100\ \Omega$.

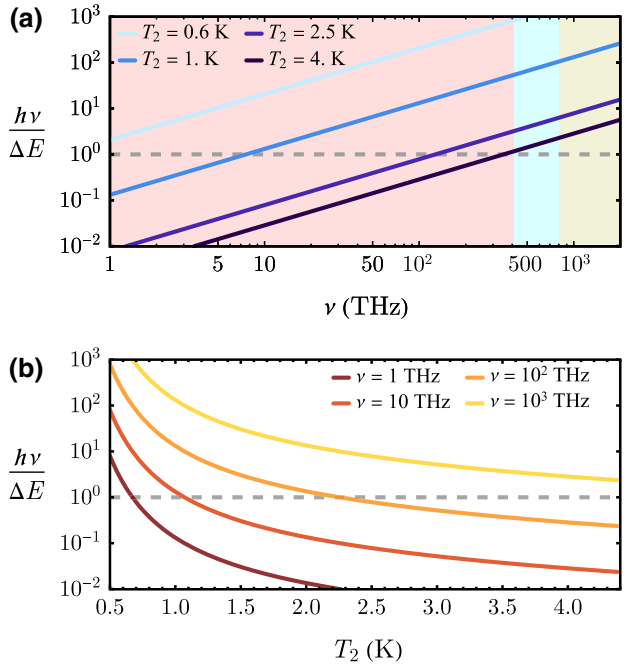

FIG. 9. (a) The resolving power as a function of the photon frequency at a few temperatures. The shaded regions indicate the frequency ranges corresponding to IR (red), visible (cyan), and UV (green) light spectra. (b) The resolving power as a function of the temperature at a few values of the photon frequency. The values of other parameters are as follows: $V_2 = 0.01\ \mu\text{m}^3$, $T_{c_2} = 4.4$ K, and $N_{F,2} = 10^{47}\ \text{J}^{-1}\ \text{m}^{-3}$.

The temperature dependence of the resolving power at a few values of the photon frequency is shown in Fig. 9(b). We note that the resolving power reduces monotonically with an increase in the temperature and that the higher the value of ν, the larger is the range of temperatures giving $h\nu/\Delta E > 1$.

We estimate the sensitivity of the device by assuming some thermal response to the photon absorption. However, we need to discuss how critical-current measurements can be undertaken without affecting the previous conclusions. Reading of the photon-induced I_c variation could be performed by conventional techniques, for instance, via a Josephson sensor [61] based on modifications of the kinetic inductance, $L_k \propto 1/I_c$ [25,26], of the junction working in the dissipationless regime and inductively coupled to a superconducting quantum-interference device (SQUID). Alternatively, the variation of the Josephson kinetic inductance of the junction can be performed dispersively through an LC (inductance-capacitance) tank circuit inductively coupled to the JJ [68,69]. As a matter of fact, in this readout scheme the modifications of the Josephson inductance can be measured through a shift, or a broadening, of the circuit's transmission or reflection resonance [70]. Detectors based on dispersive detection have a huge potential in fast detection and quantum-limited energy resolution [69]. Those platforms, combined with the dissipationless configuration of our tunnel junction, could promise minimal low-noise performance with reduced dark counts and, consequently, high energy sensitivity. In this dispersive configuration, one can also deploy multiplexing capabilities, paving the way for the real-time control of more single-photon sensors and making an ideal platform for astrophysical applications.

Finally, we observe that our detection proposal actually highlights some similarities with other single-photon sensors based on the critical-current change due to photon absorption in a proximized nanowire [52,55,57,69]. There are also several qualifying differences. First, in our detection scheme, the absorbing element is a superconducting lead of an asymmetric JJ and the phenomenon exploited for the detection is the anomalous steep variation brought about by changing the temperature of the critical current, where its temperature variation is smoother in proximized sensors. Therefore, the strength of our device lies in a strong sensitivity due to the steeplike response of I_c to photon-induced heating. Moreover, the fact that the detection is not performed in extremely low-temperature regimes could be advantageous for achieving a fast thermal response due to a better e-ph coupling, which results in a shorter dead time of the detector. Markedly, we think that our detector represents an interesting combination of different types of superconducting single-photon and calorimetric devices. In particular, it has the potential sensitivity of STJ systems, but without being affected by Johnson-Nyquist noise, due to the dissipationless working regime. Besides, the proposed detector potentially has the energy sensitivity of proximity-based detectors, with a reduced dead time at parity of photon energy, due to higher operating temperatures. Finally, it is characterized by a fast thermal response, due to the energy absorption with a short timing jitter, similar to the case of transition-edge sensors. In conclusion, we wish to stress that the presented analysis is not specifically optimized with regard to performance but is simply done on the basis of realistic and feasible parameters. We will present a more detailed analysis of both the detector design and its performance figures of merit in a forthcoming paper [71].

Before concluding, we wish to remark that our prediction of a jump in the critical current, in the presence of both an asymmetry of the junction and a temperature bias, is purely based on a conventional BCS mechanism, i.e., the matching of gaps. This means that for all those experiments where jumps in the critical current are indeed discussed as a smoking-gun proof of more elaborate mechanisms, such as, for instance, topological transitions [72–74], one needs to take extra care in order to be sure that structural asymmetry, in the presence of an uncontrolled evolution of the thermal gradient, could eventually provide a simpler explanation.

V. CONCLUSIONS

In this paper, we discuss the behavior of the critical current, I_c, of a Josephson tunnel junction formed by different superconductors. We analyze in detail the behavior of I_c by changing both the temperatures of the electrodes and the ratio, r, between the critical temperatures of the superconductors. We observe that the critical current is asymmetric in response to a temperature switching and that it shows steeplike behavior at specific temperatures, namely, at the temperatures at which the BCS superconducting gaps coincide. Specifically, in these conditions the critical current of an asymmetric junction, i.e., $r \neq 1$, suddenly jumps. We also observe unexpected behavior, since, for $r > 1$, the critical current corresponding to a jump increases with an increase in temperature.

Studying the height of the I_c jump, we observe nonmonotonic behavior, according to which we find that an optimal r value exists, which gives a maximum increase of the critical current upon variation of the temperature. We also discuss how the values of the Dynes parameter in the superconductors affect the sharpness of the I_c transition. Finally, we discuss in detail the behavior of the critical current for a small thermal gradient along the junction as a function of the average temperature and the values of the Dynes parameter.

The distinctive temperature dependence of the critical current of an asymmetric Josephson junction can be relevant for the conception of intriguing applications. For instance, the steplike variation with temperature of the critical current will allow us to design a single-photon threshold detector in which the absorption of a photon produces a temperature enhancement, which can correspond to a measurable critical-current variation. This system operating in the nondissipative branch is likely to provide very-high-energy sensitivity. The conceived device is inherently energy resolving and can be also engineered to determine the photon number in the case of a monochromatic source of light. We briefly discuss the essential figures of merit of this type of detector, which deserve further investigation and more careful design optimization, in order to better address its intrinsic potential [71].

ACKNOWLEDGMENTS

This research was supported in part by the National Science Foundation under Grant No. NSF PHY17-48958. C.G., A.B., and F.G. acknowledge the European Research Council under the European Unions Seventh Framework Program (No. FP7/2007-2013)/ERC Grant Agreement No. 615187-COMANCHE and the Tuscany Region under the framework funding programme PAR FAS 2007-2013, FAR-FAS 2014 call, project SCIADRO, for financial support. P.S. and A.B. have received funding from the European Union FP7/2007-2013 under REA Grant Agreement No. 630925—COHEAT. A.B. acknowledges the CNR-CONICET cooperation program "Energy conversion in quantum nanoscale hybrid devices" and the Royal Society through the International Exchanges between the UK and Italy (Grant No. IES R3 170054).

[1] B. D. Josephson, Possible new effects in superconductive tunnelling, Phys. Lett. **1**, 251 (1962).
[2] P. W. Anderson, and J. M. Rowell, Probable Observation of the Josephson Superconducting Tunneling Effect, Phys. Rev. Lett. **10**, 230 (1963).
[3] F. Giazotto, and M. J. Martńez-Pérez, The Josephson heat interferometer, Nature **492**, 401 (2012).
[4] M. J. Martńez-Pérez, and F. Giazotto, A quantum diffractor for thermal flux, Nat. Commun. **5**, 3579 (2014).
[5] M. J. Martínez-Pérez, P. Solinas, and F. Giazotto, Coherent caloritronics in Josephson-based nanocircuits, J. Low Temp. Phys. **175**, 813 (2014).
[6] A. Fornieri, and F. Giazotto, Towards phase-coherent caloritronics in superconducting circuits, Nat. Nanotechnol. **12**, 944 (2017).
[7] K. Maki, and A. Griffin, Entropy Transport Between Two Superconductors by Electron Tunneling, Phys. Rev. Lett. **15**, 921 (1965).
[8] F. Giazotto, T. T. Heikkilä, A. Luukanen, A. M. Savin, and J. P. Pekola, Opportunities for mesoscopics in thermometry and refrigeration: Physics and applications, Rev. Mod. Phys. **78**, 217 (2006).
[9] M. Meschke, W. Guichard, and J. P. Pekola, Single-mode heat conduction by photons, Nature **444**, 187 (2006).
[10] F. Giazotto, and M. J. Martńez-Pérez, Phase-controlled superconducting heat-flux quantum modulator, Appl. Phys. Lett. **101**, 102601 (2012).
[11] F. Giazotto, M. J. Martńez-Pérez, and P. Solinas, Coherent diffraction of thermal currents in Josephson tunnel junctions, Phys. Rev. B **88**, 094506 (2013).
[12] C. Guarcello, F. Giazotto, and P. Solinas, Coherent diffraction of thermal currents in long Josephson tunnel junctions, Phys. Rev. B **94**, 054522 (2016).
[13] M. J. Martńez-Pérez, A. Fornieri, and F. Giazotto, Rectification of electronic heat current by a hybrid thermal diode, Nat. Nanotechnol. **10**, 303 (2015).
[14] Antonio Fornieri, Giuliano Timossi, Riccardo Bosisio, Paolo Solinas, and Francesco Giazotto, Negative differential thermal conductance and heat amplification in superconducting hybrid devices, Phys. Rev. B **93**, 134508 (2016).
[15] C. Guarcello, P. Solinas, M. Di Ventra, and F. Giazotto, Hysteretic Superconducting Heat-Flux Quantum Modulator, Phys. Rev. Appl. **7**, 044021 (2017).
[16] C. Guarcello, P. Solinas, M. Di Ventra, and F. Giazotto, Solitonic Josephson-based meminductive systems, Sci. Rep. **7**, 46736 (2017).
[17] C. Guarcello, P. Solinas, A. Braggio, M. Di Ventra, and F. Giazotto, Josephson Thermal Memory, Phys. Rev. Appl. **9**, 014021 (2018).
[18] P. Solinas, R. Bosisio, and F. Giazotto, Microwave quantum refrigeration based on the Josephson effect, Phys. Rev. B **93**, 224521 (2016).

[19] F. Paolucci, G. Marchegiani, E. Strambini, and F. Giazotto, Phase-Tunable Thermal Logic: Computation with Heat, Phys. Rev. Appl. **10**, 024003 (2018).

[20] G. F. Timossi, A. Fornieri, F. Paolucci, C. Puglia, and F. Giazotto, Phase-tunable Josephson thermal router, Nano Lett. **18**, 1764 (2018).

[21] C. Guarcello, P. Solinas, A. Braggio, and F. Giazotto, Solitonic Josephson Thermal Transport, Phys. Rev. Appl. **9**, 034014 (2018).

[22] F. Paolucci, G. Marchegiani, E. Strambini, and F. Giazotto, Phase-tunable temperature amplifier, EPL **118**, 68004 (2017).

[23] C. Guarcello, P. Solinas, A. Braggio, and F. Giazotto, Phase-coherent solitonic Josephson heat oscillator, Sci. Rep. **8**, 12287 (2018).

[24] V. Ambegaokar, and A. Baratoff, Tunneling Between Superconductors, Phys. Rev. Lett. **10**, 486 (1963).

[25] A. Barone, and G. Paternò, *Physics and Applications of the Josephson Effect* (Wiley, New York, 1982).

[26] K. K. Likharev, *Dynamics of Josephson Junctions and Circuits* (Gordon and Breach, New York, 1986).

[27] R. E. Harris, Cosine and other terms in the Josephson tunneling current, Phys. Rev. B **10**, 84 (1974).

[28] D. Golubev, T. Faivre, and J. P. Pekola, Heat transport through a Josephson junction, Phys. Rev. B **87**, 094522 (2013).

[29] F. Giazotto, T. T. Heikkilä, and F. S. Bergeret, Very Large Thermophase in Ferromagnetic Josephson Junctions, Phys. Rev. Lett. **114**, 067001 (2015).

[30] M. Tinkham, *Introduction to Superconductivity*, 2nd ed. (Dover Publications, Mineola, 2004).

[31] A. A. Golubov, M. Yu. Kupriyanov, and E. Il'ichev, The current-phase relation in Josephson junctions, Rev. Mod. Phys. **76**, 411 (2004).

[32] F. Giazotto, and J. P. Pekola, Josephson tunnel junction controlled by quasiparticle injection, J. Appl. Phys. **97**, 023908 (2005).

[33] S. Tirelli, A. M. Savin, C. Pascual Garcia, J. P. Pekola, F. Beltram, and F. Giazotto, Manipulation and Generation of Supercurrent in Out-of-Equilibrium Josephson Tunnel Nanojunctions, Phys. Rev. Lett. **101**, 077004 (2008).

[34] R. Bosisio, P. Solinas, A. Braggio, and F. Giazotto, Photonic heat conduction in Josephson-coupled Bardeen-Cooper-Schrieffer superconductors, Phys. Rev. B **93**, 144512 (2016).

[35] R. C. Dynes, V. Narayanamurti, and J. P. Garno, Direct Measurement of Quasiparticle-Lifetime Broadening in a Strong-Coupled Superconductor, Phys. Rev. Lett. **41**, 1509 (1978).

[36] R. C. Dynes, J. P. Garno, G. B. Hertel, and T. P. Orlando, Tunneling Study of Superconductivity Near the Metal-Insulator Transition, Phys. Rev. Lett. **53**, 2437 (1984).

[37] J. P. Pekola, V. F. Maisi, S. Kafanov, N. Chekurov, A. Kemppinen, Yu. A. Pashkin, O.-P. Saira, M. Möttönen, and J. S. Tsai, Environment-Assisted Tunneling as an Origin of the Dynes Density of States, Phys. Rev. Lett. **105**, 026803 (2010).

[38] O.-P. Saira, A. Kemppinen, V. F. Maisi, and J. P. Pekola, Vanishing quasiparticle density in a hybrid Al/Cu/Al single-electron transistor, Phys. Rev. B **85**, 012504 (2012).

[39] J. P. Pekola, T. T. Heikkilä, A. M. Savin, J. T. Flyktman, F. Giazotto, and F. W. J. Hekking, Limitations in Cooling Electrons using Normal-Metal-Superconductor Tunnel Junctions, Phys. Rev. Lett. **92**, 056804 (2004).

[40] J. Clarke and A. I. Braginski, *The SQUID Handbook: Fundamentals and Technology of SQUIDs and SQUID Systems*, Series The SQUID Handbook Vol. 1 (Wiley, Weinheim, 2004).

[41] A. F. Andreev, The thermal conductivity of the intermediate state in superconductors, J. Exp. Theor. Phys. **19**, 1228 (1964).

[42] We note that the sharpness of the jump depends on the value of the Dynes parameters, as we will discuss in detail later.

[43] Since the detection readout can be done in the nondissipative regime, as we will discuss later, any change in I_c does not affect the thermal exchanges.

[44] M. J. Martńez-Pérez, and F. Giazotto, Efficient phase-tunable Josephson thermal rectifier, Appl. Phys. Lett. **102**, 182602 (2013).

[45] F. Giazotto, and F. S. Bergeret, Thermal rectification of electrons in hybrid normal metal-superconductor nanojunctions, Appl. Phys. Lett. **103**, 242602 (2013).

[46] A. Fornieri, M. J. Martńez-Pérez, and F. Giazotto, Electronic heat current rectification in hybrid superconducting devices, AIP Adv. **5**, 053301 (2015).

[47] C. W. Chang, D. Okawa, A. Majumdar, and A. Zettl, Solid-state thermal rectifier, Science **314**, 1121 (2006).

[48] W. Kobayashi, Y. Teraoka, and I. Terasaki, An oxide thermal rectifier, Appl. Phys. Lett. **95**, 171905 (2009).

[49] H. Tian, D. Xie, Y. Yang, T.-L. Ren, G. Zhang, Y.-F. Wang, C.-J. Zhou, P.-G. Peng, L.-G. Wang, and L.-T. Liu, A novel solid-state thermal rectifier based on reduced graphene oxide, Sci. Rep. **2**, 523 (2012).

[50] R. Scheibner, M. König, D. Reuter, A. D. Wieck, C. Gould, H. Buhmann, and L. W. Molenkamp, Quantum dot as thermal rectifier, New J. Phys. **10**, 083016 (2008).

[51] J. Wei, D. Olaya, B. S. Karasik, S. V. Pereverzev, A. V. Sergeev, and M. E. Gershenson, Ultrasensitive hot-electron nanobolometers for terahertz astrophysics, Nat. Nanotechnol. **3**, 496 (2008).

[52] J. Voutilainen, M. A. Laakso, and T. T. Heikkilä, Physics of proximity Josephson sensor, J. Appl. Phys. **107**, 064508 (2010).

[53] Y.-F. Chen, D. Hover, S. Sendelbach, L. Maurer, S. T. Merkel, E. J. Pritchett, F. K. Wilhelm, and R. McDermott, Microwave Photon Counter Based on Josephson Junctions, Phys. Rev. Lett. **107**, 217401 (2011).

[54] K. K. Berggren, E. Dauler, A. J. Kerman, S.-W. Nam, and D. Rosenberg, in Experimental Methods in the Physical Sciences Vol. 45 (Elsevier, 2013), p. 185.

[55] P. Solinas, F. Giazotto, and G. P. Pepe, Proximity SQUID Single-Photon Detector via Temperature-to-Voltage Conversion, Phys. Rev. Appl. **10**, 024015 (2018).

[56] E. D. Walsh, D. K. Efetov, G.-H. Lee, M. Heuck, J. Crossno, T. A. Ohki, P. Kim, D. Englund, and K. C. Fong, Graphene-based Josephson-Junction Single-Photon Detector, Phys. Rev. Appl. **8**, 024022 (2017).

[57] P. Virtanen, A. Ronzani, and F. Giazotto, Josephson Photodetectors via Temperature-to-Phase Conversion, Phys. Rev. Appl. **9**, 054027 (2018).

[58] B. S. Karasik, W. R. McGrath, M. E. Gershenson, and A. V. Sergeev, Photon-noise-limited direct detector based on disorder-controlled electron heating, J. Appl. Phys. **87**, 7586 (2000).

[59] S. Chakraborty, and T. T. Heikkilä, Thermoelectric radiation detector based on a superconductor-ferromagnet junction: Calorimetric regime, J. Appl. Phys. **124**, 123902 (2018).

[60] T. T. Heikkilä, R. Ojajärvi, I. J. Maasilta, E. Strambini, F. Giazotto, and F. S. Bergeret, Thermoelectric Radiation Detector based on Superconductor-Ferromagnet Systems, Phys. Rev. Appl. **10**, 034053 (2018).

[61] F. Giazotto, T. T. Heikkilä, G. P. Pepe, P. Helistö, A. Luukanen, and J. P. Pekola, Ultrasensitive proximity Josephson sensor with kinetic inductance readout, Appl. Phys. Lett. **92**, 162507 (2008).

[62] A. Peacock, P. Verhoeve, N. Rando, A. Van Dordrecht, B. G. Taylor, C. Erd, M. A. C. Perryman, R. Venn, J. Howlett, and D. J. Goldie *et al.*, Single optical photon detection with a superconducting tunnel junction, Nature **381**, 135 (1996).

[63] A. Peacock, P. Verhoeve, N. Rando, A. van Dordrecht, B. G. Taylor, C. Erd, M. A. C. Perryman, R. Venn, J. Howlett, D. J. Goldie, J. Lumley, and M. Wallis, On the detection of single optical photons with superconducting tunnel junction, J. Appl. Phys. **81**, 7641 (1997).

[64] T. Peacock, P. Verhoeve, N. Rando, C. Erd, M. Bavdaz, B. G. Taylor, and D. Perez, Recent developments in superconducting tunnel junctions for ultraviolet, optical & near infrared astronomy, Astron. Astrophys. Suppl. Ser. **127**, 497 (1998).

[65] In the presence of the thermal gradient, there will be a quasiparticle-heat-current diffusion between the two superconductors but, due to particle-hole symmetry, there is no thermoelectric current associated with it.

[66] F. Brange, P. Samuelsson, B. Karimi, and J. P. Pekola, Nanoscale quantum calorimetry with electronic temperature fluctuations, Phys. Rev. B **98**, 205414 (2018).

[67] H. Rabani, F. Taddei, O. Bourgeois, R. Fazio, and F. Giazotto, Phase-dependent electronic specific heat of mesoscopic Josephson junctions, Phys. Rev. B **78**, 012503 (2008).

[68] J. Govenius, R. E. Lake, K. Y. Tan, V. Pietilä, J. K. Julin, I. J. Maasilta, P. Virtanen, and M. Möttönen, Microwave nanobolometer based on proximity Josephson junctions, Phys. Rev. B **90**, 064505 (2014).

[69] J. Govenius, R. E. Lake, K. Y. Tan, and M. Möttönen, Detection of Zeptojoule Microwave Pulses Using Electrothermal Feedback in Proximity-Induced Josephson Junctions, Phys. Rev. Lett. **117**, 030802 (2016).

[70] P. K. Day, H. G. LeDuc, B. A. Mazin, A. Vayonakis, and J. Zmuidzinas, A broadband superconducting detector suitable for use in large arrays, Nature **425**, 817 (2003).

[71] C. Guarcello, A. Braggio, P. Solinas, G. P. Pepe, and F. Giazotto, Josephson threshold calorimeter, arXiv:1901.01456.

[72] P. Marra, R. Citro, and A. Braggio, Signatures of topological phase transitions in Josephson current-phase discontinuities, Phys. Rev. B **93**, 220507 (2016).

[73] J. Tiira, E. Strambini, M. Amado, S. Roddaro, P. San-Jose, R. Aguado, F. S. Bergeret, D. Ercolani, L. Sorba, and F. Giazotto, Magnetically-driven colossal supercurrent enhancement in InAs nanowire Josephson junctions, Nat. Commun. **8**, 14984 (2017).

[74] J. Cayao, P. San-Jose, A. M. Black-Schaffer, R. Aguado, and E. Prada, Majorana splitting from critical currents in Josephson junctions, Phys. Rev. B **96**, 205425 (2017).